Research Article / Review Article

FUPRE JOURNAL 10(2):18-37(2026)
https://doi.org//10.60787/FJSIR.v10i2.18-37

FUPRE Journal
of
Scientific and Industrial Research

ISSN: 2579-1184(Print) ISSN: 2578-1129 (Online)

http://fupre.edu.ng/journal

First Principles Assessment of Structural, Electronic, and Thermoelectric Properties of KTiAl and KYC for Energy Conversion Applications

AGBAWE, O. N. *, *NENUWE, O. N.*

Department of Physics, Federal University of Petroleum Resources, 1221, Effurun, Nigeria

ARTICLE INFO

Received: 22/04/2026
Accepted: 17/08/2026

Keywords

DFT,
Electronic properties,
KTiAl, KYC,
Thermoelectric properties

ABSTRACT

Half-Heusler materials are promising candidates for thermoelectric devices that could help alleviate the current global energy crisis by converting waste thermal energy into electricity. This study presents a systematic computational assessment of the structural, electronic, mechanical, and thermoelectric properties of KTiAl and KYC half-Heusler compounds using density functional theory (DFT) and semi-classical Boltzmann transport theory implemented via the WIEN2k computational code and BoltzTraP2 software. The PBE-GGA and modified Becke-Johnson (mBJ) exchange-correlation approximations were employed for the calculations. Volume optimization calculations carried out across the α, β, and γ atomic configurations reveal that the type-α phase is the energetically most stable configuration for both compounds. Elastic parameters confirm that both materials satisfy the Born stability criteria and exhibit strong metallic-like ductility, supported by a Pugh ratio B/G > 1.75 and a positive Cauchy pressure. Electronic structures evaluated via the mBJ functional reveal that both alloys are non-magnetic, direct-bandgap semiconductors, with narrow bandgaps of 0.15 eV for KTiAl and 0.84 eV for KYC. Thermoelectric transport coefficients demonstrate a significant dependence on absolute temperature (T) and chemical potential (μ). Incorporating lattice thermal conductivity calculated via Slack's equation, the figure of merit (ZT) at optimal carrier concentration elevates from ambient temperature values (0.31 for KTiAl; 0.18 for KYC) to high mid-temperature peaks of 0.81 for KTiAl and 0.61 for KYC at 700 K. These findings establish that KTiAl and KYC are mechanically ductile, stable, and highly efficient semiconductors optimized for medium-to-high-temperature clean energy harvesting and waste-heat recovery applications.

1. INTRODUCTION

The energy crisis is a worldwide problem, and if we don't take steps to generate alternate sources of energy, things will get progressively worse in the years to come (Coyle & Simmons, 2014; Ole Rolser Christer Tryggestad, 2019). Although fossil fuels are the main source of energy, systems that use them usually have an efficiency of just about 40% or below 40%, with the remaining energy coming in the form of waste. Reducing harmful emissions and addressing economic and environmental issues require a shift away from non-renewable energy sources. It is crucial to develop energy resources to lessen the world's energy constraint and encourage sustainable growth (Khaliq *et al.*, 2024; Xu *et al.*, 2024). Consequently, converting this waste heat into valuable electrical energy would help to mitigate the energy problem. Based on the Seebeck phenomenon, thermoelectric (TE) devices are made to transform thermal energy into electrical energy for waste heat recovery (Seebeck, 2003). A dimensionless figure

*Corresponding author, e-mail: nenuwe.nelson@fupre.edu.ng
https://doi.org/10.60787/FJSIR.v10i2.18-37
©Scientific Information, Documentation and Publishing Office at FUPRE Journal

of merit (Z_T) is used to quantify a thermoelectric device's performance. In terms of mathematics, it is expressed as

$$Z_T = \left(\frac{S^2\sigma T}{\kappa_l + \kappa_e}\right) \quad (1)$$

Where S is the Seeback coefficient, κ_l stands for lattice thermal conductivity, κ_e represents electronic thermal conductivity, and T is the absolute temperature (Chand *et al.*, 2025). It is difficult to simultaneously increase the power factor ($S^2\sigma$) and decrease thermal conductivity in order to maximize Z_T values due to the interplay of the Seebeck coefficient, electrical conductivity, and electronic thermal conductivity (Zhang & Zhao, 2015). Optimizing the figure of merit has continued to be the focus in the development of thermoelectric devices and materials. In the realm of thermoelectricity, various material types have been investigated for their possible uses. These include PbTe (Sharma *et al.*, 2021), skutterudites (Rogl & Rogl, 2017), chalcogenides (Shi *et al.*, 2019), transition-metal-tellurides (Tritt *et al.*, 2001), antimonides (Guo *et al.*, 2025), and half-Heusler compounds (Subramani *et al.*, 2025).

Half-Heusler (HH) compounds are gaining attention for their possible use in thermoelectric devices (Nenuwe & Yebovi, 2024), particularly for recovering waste heat from industries, cars, and residential heating systems at medium to high temperatures. HH compounds are ternary inter-metallics defined by the chemical formula XYZ, where X and Y are transition metals and Z is a p-block element. They have a face-centered cubic (FCC) structure with Wyckoff positions of (0,0,0), (1/4,1/4,1/4), and (1/2,1/2,1/2). HH compounds with 18 valence electrons are non-magnetic semiconductors with outstanding electrical properties, high thermal stability, improved Z_T values, and mechanical resilience, making them a viable material for high thermoelectric efficiency (Al-Douri & Ameri, 2025; Nenuwe & Omagbemi, 2026; Saikia *et al.*, 2025). The optoelectronic and photocatalytic response of half-Heusler compounds KXP (X = Ba, Ca, Sr) were examined by Hashmat and his team (Hashmat *et al.*, 2025) employing the density functional theory (DFT)). They discovered that these alloys are direct band gap semiconductors with band gaps that range between 1.78 and 2.37 eV, making them promising materials for visible-light-driven applications. They were noticed to exhibit high absorption coefficients of 1.52 x 10^6cm^{-1} for KCaP, 1.30 x 10^6cm^{-1} for KSrP, and 1.24 x 10^6cm^{-1} for KBaP, respectively. In a study on the HH alloys, such as KScGe, KTiGa, and KVAs, Özdoğan and his colleague found that K-based compounds KZ(Ga, Ge, As, Se) with Z representing transition metal (Özdoğan & Galanakis, 2024), show half-metallicity that makes them suitable for spintronic applications. The thermoelectric and UV protection applications of KCaAs and KCaP were investigated by Hammadache *et al.*, with maximum Z_T value of 0.77 for both compounds (Hammadache *et al.*, 2024). Shrivastava & Sanyal (Shrivastava & Sanyal, 2019) theoretically investigated the thermoelectric, phonon and electronic properties of KYX (X=Si and Ge) and KScX (X=Sn and Pb) alloys with valence electron count (VEC) of 8. They found these compounds to be a direct band gap semiconductors with values ranging between 0.27 and 0.50 eV. The phonon dispersion reveals dynamical stability, and thermoelectric properties show high power factor.

Gruhn *et al.* (Gruhn, 2010a) presents a high-throughput DFT study of 648 half-Heusler compounds, screening for non-toxic materials with desirable structural and electronic properties. The study provides a foundational database, predicting structural stability and band gaps across five chemical families to accelerate material discovery for optoelectronic applications. The KTiAl and KYC half-Heusler compounds were among the materials studied. However,

the study only provided data on the lattice constant for KTiAl and KYC alloys. Recently, the fundamental physical properties of alkali-yttrium half-Heusler alloys KYC, RbYC, and CsYC were investigated (Achir *et al.*, 2026). Using Density Functional Theory (DFT), the researchers evaluate whether these materials are practically viable for photovoltaic, optoelectronic, and high-temperature thermoelectric applications.

Following the research trend in the literature, we have observed that information on the experimental and theoretical reports for these two compounds is very scarce. There is no report on the electronic, optical, mechanical, and thermoelectric properties of potassium titanium aluminium (KTiAl), whereas, for potassium yttrium carbon (KYC), only one theoretical study has been reported on the physical properties (Achir *et al.*, 2026). The study by Achir *et al.* relies on GGA functionals, which likely underestimate bandgaps.

Therefore, this work provides information on the structural, thermoelectric, electronic, and mechanical properties of KTiAl and KYC half-Heusler alloys. We adopt the first principles calculations based on density functional theory (DFT) as configured in the Wien2k software package and the BoltzTrap2 computational code.
The selection of these materials is justified by their potential to act as novel, low-cost, environmentally friendly semiconductors with exceptional energy-conversion and optoelectronic properties. Furthermore, potassium (K) was chosen for its high electro-positivity and wide ionic radius, enabling systematic tweaking of half-Heusler alloys' electronic structure and band characteristics, which are crucial parameters in thermoelectric optimization (Khatri *et al.*, 2026). Combining high atomic mass materials (such as Ti and Y) boosts phonon scattering, reducing thermal conductivity and improving thermoelectric performance (Gurunani & Gupta, 2025a). Also, as noted by materials experts, half-Heusler alloys, including those with 8-valence electrons are recognized for their ability to convert waste heat into electricity.

This paper is structured as follows: the computational methods are covered in Section 2, the key results and discussion are covered in Section 3, and the conclusion of the research is presented in the final section.

2. MATERIALS AND METHODS

Using first-principles calculation and the Full Potential-Linearized Augmented-Plane Wave (FP-LA-PW) tool from the DFT-based Wien2k simulation program, we examined the interaction between atomic valence and core electrons (Blaha *et al.*, 2020; Schwarz *et al.*, 2002). To determine the electronic properties, we used the functional PBE-GGA (Haro, 2025; Wu & Cohen, 2006) and mBJ (Tran & Blaha, 2009). The most accurate method for determining a solid's electronic structure is Wien2k. The Wien2k software uses the FP-LA-PW approach to solve the self-consistent Kohn-Sham equations (Kumar & Chand, 2023; Panday *et al.*, 2026).

$$\left(\frac{\hbar^2}{2m}\nabla^2 - V_{eff}(r)\right)\varphi_i(r) = \varepsilon_i\,\varphi_i(r) \quad (2)$$

Where ε_i stands for the orbital energy of the equivalent Kohn-Sham orbital φ_i. For a system with N particles, the electron density ρ(r) is determined by

$$\rho(r) = \sum_{i}^{N} |\varphi_i(r)|^2 \quad (3)$$

Potential and charge density are used in several ways in the FP-LAPW method.

$$V(r) = \sum_{lm} V_{lm}\, Y_{lm}(r) \quad (4)$$

$$V(r) = \sum_{k} V_k\, e^{ikr} \quad (5)$$

Eqs. (4) and (5) stand for internal and external of a muffin-tin ball. The Y_{lm}

represents spherical harmonics. For an effective convergence set in the first Brillouin zone, the following parameters were employed: $R_{MT}K_{max}$ = 8, k-points = 2,000, and cut-off energy = -6.0 Ry. The KTiAl muffin-tin radii (R_{MT}) are 2.24, 2.36 and 2.13 for K, Ti and Al. For KYC, the R_{MT} are 2.36, 2.47 and 2.02 for K, Y, and C, respectively. To ensure self-consistency in the simulation, the energy convergence was adjusted to 10^{-5} Ry and charge convergence to 10^{-4} e. Additionally, the G_{MAX} parameter was set to 12, and spherical harmonics inside the atomic spheres were expanded using a maximum quantum number of l_{max}=10. The BoltzTrap code uses semi-classical Boltzmann transport theory to determine the thermoelectric properties such as Seebeck coefficient (S), electrical conductivity (σ/τ), electronic thermal conductivity (κ_e/τ), and power factor ($S^2\sigma/\tau$) (Madsen *et al.*, 2018). A constant relaxation time approximation (CRTA) was used for the computations. We assume in CRTA that the relaxation time τ is constant at all chemical potentials and temperatures. For every temperature and chemical potential, the transport coefficients were computed. The electronic transport properties were then used to calculate the figure of merit (Z_T) parameter, ignoring the lattice thermal conductivity. For the thermoelectric properties' calculations, a denser mess of (27 x 27 × 27) k-points was used. In order to determine the dynamical stability of KTiAl and KYC, phonon calculations were performed using a 2 x 2 x 2 q-mesh in the phonon Brillouin zone using the density functional perturbation theory implemented in Quantum Espresso within the PBE-GGA exchange-correlation functional (Baroni *et al.*, 2009).

3. RESULTS AND DISCUSSION

This section will describe the computational findings for the various physical properties of the KTiAl and KYC half-Heusler compounds.

3.1 Structural properties of KTiAl and KYC

The general formula for half-Heusler compounds is XYZ, where X and Y belong to the rare-earth or transition elements, and Z is a member of the main group of the periodic table. These compounds crystalize in non-centrosymmetric cubic FFC structure and F-43m space group no. 216. Three types of crystal structures: α, β, and γ type are possible, depending on how the atoms (XYZ) are arranged on the Wyckoff atomic positions. For the α, β, and γ types in the KTiAl and KYC combination, Table 1 shows the Wyckoff atomic locations. Volume optimization calculations were carried out in the three structural phases, and it reveals that phase type-α of KTiAl and KYC has the lowest energy and is the most stable when compared to the beta (β) and gamma (γ) type as shown in Figure 1. Non-spin-polarized calculations were executed for both materials. The structural optimized properties such as bulk modulus (B), lattice constant (a_0) and the pressure derivatives of bulk modulus (B') are determined by calculating the total energy of the compounds as a function of the volume unit cell and fitted to the Murnaghan equation presented in Eq. (6) (Murnaghan, 1944; Tyuterev & Vast, 2006).

$$\boldsymbol{E_T(V) = -\frac{B_0 V}{\acute{B}_0(\acute{B}_0 - 1)}\left\{\left(1 - \left(\frac{V_0}{V}\right)^{\acute{B}_0}\right) - \acute{B}_0\left(\frac{V_0}{V} - 1\right)\right\} + E_0}, \quad (6)$$

here B_0 is bulk modulus, V_0 is volume at zero pressure, E_0 is the equilibrium total energy, and $\acute{B}_0 = \partial B_0/\partial p$. As reported in Table 2, the calculated values of the lattice parameters: a_0, B, V_0, B' & E_T for KTiAl and KYC half-Heusler within type-α phase, obtained employing the GGA+PBE, conform with other similar materials. The calculated values for a_0 agrees with previously reported data (Gruhn, 2010b). There are no

experimental results available to compare B and B'.

Table 1. The Wyckoff atomic configuration for KTiAl and KYC half-Heusler compounds.

Phase	X (= K)	Y (= Ti. Y)	Z (= Al, C)
α	0, 0, 0	0.5, 0.5, 0.5	0.25, 0.25, 0.25
β	0.5, 0.5, 0.5	0.25, 0.25, 0.25	0, 0, 0
γ	0.25, 0.25, 0.25	0, 0, 0	0.5, 0.5, 0.5

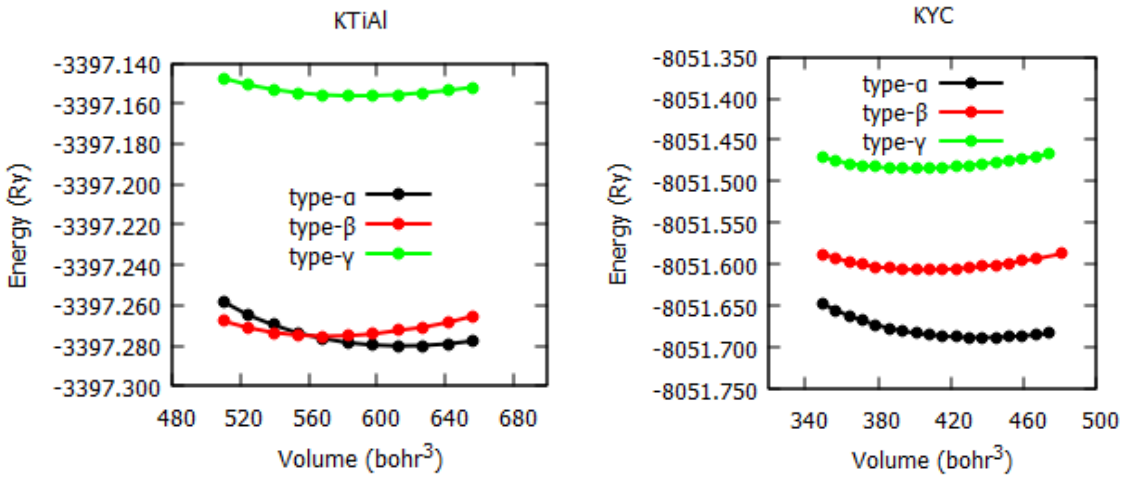


Figure 1. Total energy as a function of volume for the α, β, and γ types of KTiAl and KYC.

Table 2. Calculated lattice parameters for KTiAl and KYC.

Compound	Atom	Atomic position	Lattice constant (a_0)	Equilibrium volume (a.u.^{3})	B	B'	Band gap (eV)
KTiAl	K	(0, 0, 0)	7.14 7.14 [R1]	615.08	25.14	4.17	0.00 (PBE) 0.15 (mBJ)
	Ti	(0.5, 0.5, 0.5)					
	Al	(0.25, 0.25, 0.25)					
KYC	K	(0, 0, 0)	6.37 6.39 [R1]	435.44	48.78	3.87	0.07 (PBE) 0.84 (mBJ)
	Y	(0.5, 0.5, 0.5)					
	C	(0.25, 0.25, 0.25)					

*R1 = (Gruhn, 2010b)

3.2 Electronic properties of KTiAl and KYC

This research studies the electronic band structure (EBS), partial density of states

(PDOS) and total density of states (TDOS). Figure 2 illustrates the electronic band plots of KTiAl and KYC compounds along the high symmetry points. We first determined the energy band gap before examining the material's electronic band structures. Furthermore, the electronic structure is used to compute the transport properties. Consequently, the KTiAl compound displays a metallic character, but KYC shows a narrow band gap semiconducting nature with the PBE-GGA correlation functional, reported in Table 2. However, with the mBJ (modified Becke-Johnson) exchange-correlation potential, both materials, KTiAl and KYC behave like semiconductors with direct band gap of 0.15 eV and 0.84 eV, respectively. It is well known that the mBJ approach is a highly successful semi-local exchange-correlation potential in Density Functional Theory (DFT), developed by Tran and Blaha (Abu-Farsakh & Qteish, 2022; Tran & Blaha, 2009). Widely used in solid-state physics, it is specifically renowned for predicting highly accurate electronic band gaps in semiconductors and insulators at a fraction of the computational cost of hybrid functionals or GW.

The band gap data obtained for KYC (0.84 eV) using mBJ approximation compares well with the value reported by Achir *et al.* This value is noticed to be a bit higher. The difference may be because of the different approximations. They employed the PBE-GGA in calculating the band gap values. It is well known that the PBE-GGA method underestimate band gap values. The small energy band gap observed in this work is significant, because it enables high thermoelectric performance by enhancing electrical conductivity and optimizing the power factor at high temperatures. Additionally, these narrow gaps allow for infrared (IR) light absorption, making the materials suitable for photodetectors and sensors (Casper *et al.*, 2012; Mahmud *et al.*, 2024; Park *et al.*, 2025).

The total density of states (TDOS) and partial density of states (PDOS) have been examined and reported in Figure 3. This will enable us to determine the transport and optical properties of the materials. The TDOS and PDOS of KTiAl and KYC are investigated in energy range of -2.0 eV to 4.0 eV. The tiny vertical line represents the Fermi energy level (E_F). The right zone of E_F represents the conduction band (CB), whereas the left part represents the valence band (VB). The results for the TDOS and PDOS confirm the semiconducting characteristics of KTiAl and KYC compounds since the bands do not overlap with the E_F. The majority contribution to the band gap of KTiAl is the Ti-d state, while minority contribution comes from Al-p state. For KYC, the majority and minority contributions come from Y-d and C-p states, respectively.

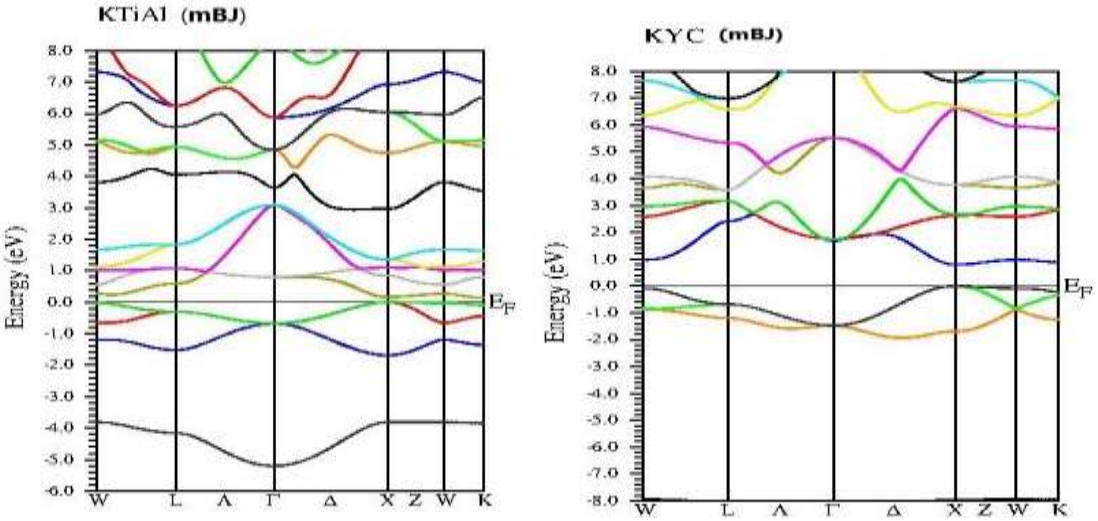


Figure 2. Electronic band structure of KTiAl and KYC compounds

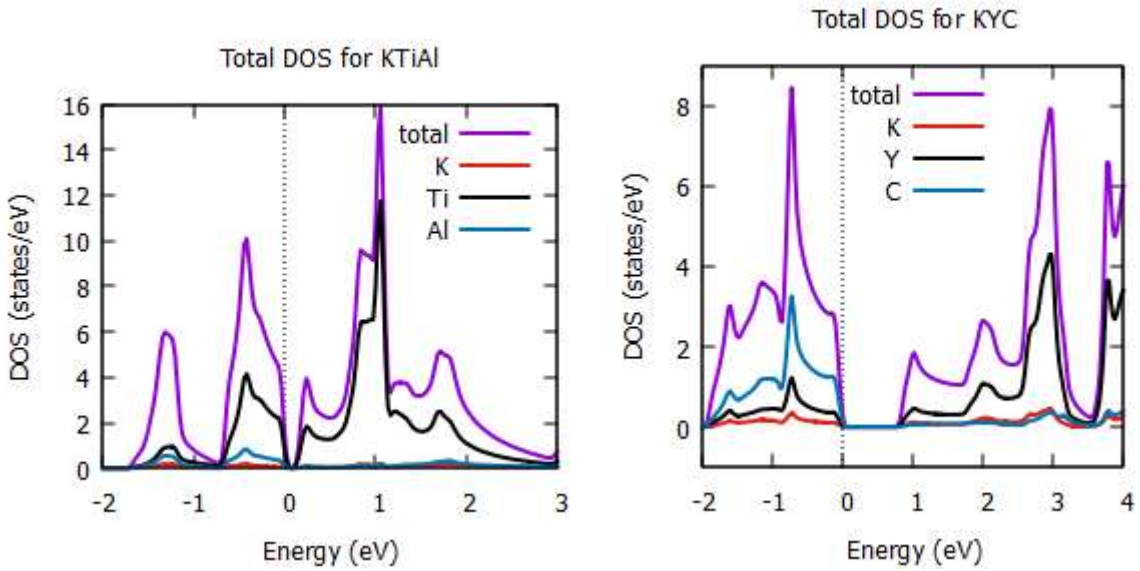


Figure 3. Total density of states of KTiAl and KYC compounds.

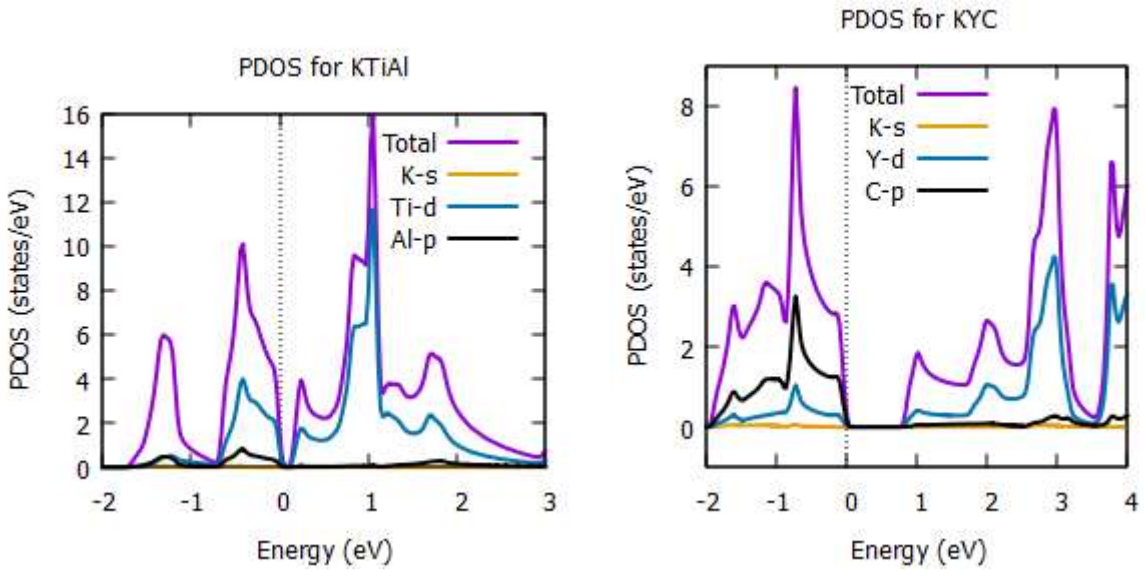


Figure 4. Partial density of states of KTiAl and KYC compounds.

Table 3. Computed values of elastic quantities $C_{11}, C_{12}, C_{44}, C_p, B, G, Y$) in GPa, Poisson's ratio ($\boldsymbol{\sigma}$), Pugh's ratio (B/G), sound velocities in (m/s), Debye temperature (Θ_D) in Kelvin and Anisotropy factor (A).

Quantity	KTiAl	KYC
$\boldsymbol{C_{11}}$	38.11	114.78
$\boldsymbol{C_{12}}$	20.50	15.32
$\boldsymbol{C_{44}}$	15.80	8.98
B	26.37	48.47
G	12.50	19.29
Y	32.37	51.09
$\boldsymbol{C_p}$	17.61	99.46
B/G	2.11	2.51
$\boldsymbol{\sigma}$	0.295	0.324
A	1.79	0.18
$\boldsymbol{V_l}$	4595.74	4547.26
$\boldsymbol{V_t}$	2476.61	2318.69
$\boldsymbol{V_m}$	2764.71	2598.06
$\boldsymbol{\Theta_D}$	262.14	277.74
Gruneisen parameter (γ)	1.74	1.93

3.3 Mechanical properties of KTiAl and KYC

Elastic parameters, which assess the relationship between strain and stress, define a material's mechanical properties. These parameters govern the material's deformation due to external forces and its subsequent return to its initial condition. Elastic constants are crucial for assessing mechanical stability, particularly in optimized conditions. The mechanical characteristics of solids, fundamental to their practical uses, are intricately linked to these elastic constants (Meneghini *et al.*, 2021). Taking into account the stability of KTiAl and KYC in the cubic α -type structure, we calculated the values of three independent elastic constants (C_{11}, C_{12}, and C_{44}). C_{11} measures longitudinal expansion, while C_{12} assesses transverse deformation. To ensure mechanical stability, the independent elastic parameters must conform to the Born stability criteria (Morris & Krenn, 2000) for cubic symmetry, as specified in Eq. (3).

$$\boldsymbol{C_{44} > 0; C_{11} > -2C_{12}; C_{12} < C_{11}; \quad C_{12} > 0;\ C_{11} > 0} \qquad (7)$$

Table 3 illustrates that the half-Heusler compounds KTiAl and KYC unequivocally meet the Born stability criterion, hence confirming their

significant mechanical stability. Moreover, the table presents additional pertinent elastic parameters, including the bulk modulus (B) and shear modulus (G), which characterize stiffness and compressibility. The B and G factors serve as indicators of the capacity to withstand plastic deformation, which quantifies the resistance to fracture. The subsequent equations are employed to ascertain the value of these quantities.

$$\boldsymbol{B = \frac{1}{3}(C_{11} + 2C_{12})} \quad (\mathbf{8})$$

$$G_V = \frac{1}{5}(C_{11} - C_{12} + 3C_{44}) \quad (9)$$

$$G_R = \frac{5C_{44}(C_{11} - C_{12})}{3(C_{11} - C_{12}) + 4C_{44}} \quad (10)$$

$$G = \frac{G_V + G_R}{2} \quad (11)$$

The indices V and R denote the Voigt and Reuss boundaries, respectively. The predicted values of these elastic parameters are presented in Table 3. The calculated data not only validates the mechanical stability of the KTiAl and KYC compounds, but they also provide valuable insights into their resistance to deformation and potential applications in various engineering and structural contexts.

The B value for KTiAl derived from Eq. (8) is roughly 4.7% greater than the value determined through structural property assessments. Whereas for KYC, the B value derived from Eq. (8) is lower than the value determined through structural property evaluation. The subsequent equation was employed to determine Young's modulus (Y), which indicates the rigidity of a material and its stress-to-strain ratio:

$$\boldsymbol{Y = \frac{9BG}{3B + G}} \quad (\mathbf{12})$$

This correlation provides insight into the elastic properties of the material by linking B and G. The Cauchy pressure (C_p) serves as a crucial elastic parameter for assessing whether a material would undergo plastic deformation (ductile) or experience fracture (brittle). The Cauchy pressure is determined by Equation (13). If the calculated C_p is greater than zero (i.e., positive), the substance is classified as ductile, signifying that it can bend, elongate, and experience considerable plastic deformation prior to fracturing. Conversely, a negative Cauchy pressure ($C_p < 0$) signifies that the material exhibits brittleness, implying that under stress, fractures advance swiftly, leading to a clean rupture with minimal plastic deformation. Our findings demonstrate that the KTiAl and KYC half-Heusler compounds display positive Cauchy pressure, hence affirming their ductility.

$$\boldsymbol{C_p = C_{11} - C_{12}} \quad (\mathbf{13})$$

An additional essential parameter for assessing ductility in contrast to brittleness is the Pugh ratio (B/G). Typically, a B/G ratio under 1.75 indicates a brittle material, while a ratio beyond 1.75 suggests a ductile substance. The computed B/G ratios for the KTiAl and KYC alloys, as presented in Table 3, further substantiates the ductility of these substances. An essential factor influencing the assessment of material compressibility is Poisson's ratio (σ). Furthermore, this relationship, depicted as the advantageous ratio of transverse strain to axial strain, elucidates the nature of bonding forces within the alloy. The subsequent equation is employed to determine this parameter. A substance possessing a higher Poisson's ratio is typically more compressible and demonstrates enhanced ductility. Nonetheless, Poisson's ratio for the KTiAl and KYC alloys suggests that these alloys

exhibit relative incompressibility, reinforcing the idea that they are ductile and mechanically robust.

$$\boldsymbol{\sigma = \frac{3B - 2G}{6B + 2G}} \qquad (\mathbf{14})$$

A significant physical parameter is the anisotropic parameter (A), which specifies the bonding properties across different crystallographic directions and is articulated by Eq. (15). A metric of A = 1 indicates isotropic material, but values below one suggests elastic anisotropy. The findings illustrated in Table 3 demonstrate that both KTiAl and KYC exhibit anisotropic properties.

$$\boldsymbol{A = \frac{2C_{44}}{C_{11} - C_{12}}} \qquad (\mathbf{15})$$

The analysis of these elastic characteristics suggests that the KTiAl and KYC half-Heusler compounds exhibit ductility and compressibility, attributes that reinforce their mechanical stability. These traits are essential for the practical use of materials, particularly in scenarios demanding robust structural integrity under stress.

The Debye temperature (Θ_D) is a crucial attribute of solid materials, representing the temperature at which the vibrational energy of the atomic constituents in the alloy equals their thermal energy. It is calculated using the average sound speed (v_m).

$$\Theta_D = \frac{\mathrm{h}}{\mathrm{k}}\left[\left(\frac{N_A}{V}\right)\left(\frac{3\mathrm{n}}{4\pi}\right)\right]^{\frac{1}{3}} v_m \qquad (16)$$

The number of atoms in each formula unit is denoted by the variable n, k represents Boltzmann's constant, V indicates the volume of the atomic cell, h symbolizes Planck's constant, and $\boldsymbol{v_m}$ refers to the average sound velocity calculated as follows:

$$v_m = \frac{1}{3}\left(\frac{1}{v_l^3} + \frac{2}{v_s^3}\right)^{-\frac{1}{3}} \qquad (17)$$

Utilizing Navier's equation with the calculated G and B, we determined the longitudinal velocity (v_l) and shear velocity (v_s). The calculated data is displayed in Table 3. The Θ_D values for KTiAl and KYC are established as 262.14 K and 277.74 K, respectively. The vibrational energy of a material's atomic components exceeds its thermal energy when the Debye temperature elevates beyond ambient temperature.

3.4 Thermoelectric properties of KTiAl and KYC

Thermoelectric (TE) materials can transform waste thermal energy into usable electricity. This application makes TE materials more environmentally friendly, clean, and suitable for green energy applications. The effectiveness of TE materials can be determined by means of a dimensionless quantity called the figure of merit, $Z_T = \left(\frac{S^2\sigma T}{\kappa_e + \kappa_l}\right)$ where S is the Seeback coefficient, κ_l stands for lattice thermal conductivity, κ_e represents electronic thermal conductivity, and T is the absolute temperature (Chand *et al.*, 2025). Additionally, the electrical conductivity is expressed as $\sigma = ne\mu$, where μ is the charge carrier mobility, e is the electronic charge, and n is the charge carrier concentration. Therefore, in order to obtain high electrical conductivity, the mobility μ needs to be high enough, which can be accomplished by raising the

materials' temperature. The BoltzTrap2 method uses the semiclassical Boltzmann transport theory to examine the transport properties of materials. Because thermal energy is lost during the manufacture and operation of electronic equipment, thermoelectric materials are necessary for energy-efficient gadgets. One important element in improving device performance is the electronic-to-heat conductivity ratio. Thermoelectric technology is utilized for a variety of applications, this includes medical, aerospace and industrial applications, transportation, electrical, and thermostat measurement. These applications are enabled by the unique benefits of this technology.

Figure 5 shows the findings of our analysis of the behaviour of thermoelectric properties as a function of the chemical potential (μ). Figure 5(a) plots the electrical conductivity per relaxation time (σ/τ) of KTiAl and KYC against chemical potential (μ) at 300, 600, and 900 K. This feature shows the intrinsic conductivity potential based on the electronic band structure of the material and is derived from Boltzmann transport theory under the constant relaxation time approximation. The electrical conductivity σ/τ is nearly zero at 300 K in the band gap area in both compounds. This is due to the lack of charge carriers at this temperature. But as μ moves into the valence or conduction bands, peaked structures arise in the p-type (μ < 0) regions. As the temperature rises, these peaks expand and slightly decrease due to thermal spreading of the Fermi-Dirac distribution.

Thermal conductivity (κ) quantifies a substance's capacity to conduct thermal energy. This transfer is fundamentally propelled by the persistent movement of atoms, which may encompass translational, rotational, and vibrational activities. These atomic oscillations provide thermal energy via multiple processes, including electron-phonon interactions and atomic vibrations at frequencies. Both the electronic contributions and lattice oscillations have a role in the total thermal conductivity, which can be represented as the combination of electronic thermal conductivity (κ_e) and lattice thermal conductivity (κ_L). Compounds exhibiting elevated electrical conductivity typically serve as good heat conductors owing to the effective transfer of electrons.

The electronic contribution to the thermal conductivity per unit relaxation time (κ_e/τ) was computed with the BoltzTrap code. The calculated (κ_e/τ) for KTiAl and KYC at different temperatures (300, 600, and 900 K) as a function of chemical potential (μ) is shown in Figure 5(b). The electronic contribution to thermal conductivity is obtained by eliminating the constant relaxation period ($\tau = 10 \times 10^{-15}$ s) from the intrinsic band structure. Both the p-type ($\mu < 0$) and n-type ($\mu > 0$) regions of the curves exhibit peaked features. The values of the p-type peak rise sharply with increase in temperature as demonstrated by Figure 5(b).

The variation of κ_e as a function of temperature is demonstrated in Figure 5(c) for both materials. A continuous increase with temperature is noticed for both KYC and KTiAl alloys. The lattice contribution to the thermal conductivity (κ_L) was computed utilizing the Slack's equation (Slack, 1973)

$$\kappa_L = \frac{A}{\gamma^2 \mathrm{T}\, n^{\frac{2}{3}}} \bar{M} \Theta_D^3 \delta\,, \qquad (18)$$

where $\delta = (V/3)^{\frac{1}{3}}$, V is the primitive unit cell volume, Θ_D Debye temperature, $\bar{M}$ represents the average atomic mass, n denotes the number of atoms in the primitive unit cell (where n is 3 and 4 for half-Heusler and quaternary Heusler), γ is the Gruneisen parameter, T stands for absolute temperature, and A (in W-mol^{-1}kg^{-1}m^{-2}K^{-2}) represents the Slack-coefficient defined as

$$A = \frac{2.436 \times 10^{-6}}{\left(1 - \frac{0.514}{\gamma} + \frac{0.228}{\gamma^2}\right)} \qquad (19)$$

The results obtained for the lattice thermal conductivity are represented in Figure 5(c) and Table 4. For both materials, κ_{lat} is noticed to decrease with rising temperatures. At room temperature, the value of κ_L is 3.52 and 3.67 for KTiAl and KYC, respectively. The behaviour of the electronic thermal conductivity (κ_e) , lattice thermal conductivity (κ_L) , and total thermal conductivity (κ_{total}) as represented in Figure 5(c) are similar to Figure 12(b) in Ref. (Gurunani & Gupta, 2025b) for KMnSn and KMnPb half-Heusler alloys.

Figure 6(a) shows the Seebeck coefficient (S) dependency on chemical potential (μ) for three crystallographic directions (xx = yy = zz) at various temperatures (300, 600, and 900 K) for KTiAl and KYC half-Heusler compounds. The Seebeck coefficient, a vital measure of thermoelectric efficiency, is the voltage produced across a material when there is a temperature differential [35]. In this case, negative S values indicate n-type conduction dominated by electrons, while positive S values indicate p-type conduction dominated by holes (Berri, 2022). The Fermi level's placement in the band structure is determined by the chemical potential, which is represented in relation to the mid-gap state (μ=0 "eV"). As a result, μ > 0 indicates n-type doping, while μ < 0 indicates p-type doping. According to our results, the highest values in all in-plane directions (xx = yy = zz) are approximately 272.4 and -275.7 μV/K around 300K for KTiAl. Under intrinsic or slightly doped conditions, these high magnitudes of S values near the underlying Fermi level suggest an effective thermoelectric response. However, the peak |S| steadily drops as the temperature rises. At 900K, the peak |S| drops to 109.6 and -111.9 μV/K. This drop is caused by thermal smearing, a phenomenon that at higher temperatures causes the Fermi Dirac distribution to become less prominent, carrier energy distributions to expand, and the voltage gradient across the material to decrease (Ullah *et al.*, 2026). Figure 6(b) reveals that the power factor (PF) exhibits strong dependence on both chemical potential and temperature. For KTiAl, the highest PF value appears around 600 K, whereas lowest is at 300 K. In the case of KYC, the PF increase with increasing temperature.

The figure of merit (Z_T) quantifies the thermoelectric functionality of a compound, determining its effectiveness in converting thermal energy into electrical energy for energy generating or cooling uses. A high Z_T value, preferably around one (1), is beneficial for a thermoelectric generator to realize optimal functionality. Figure 7 shows the temperature-sensitive behavior of the actual values of Z_T, granting enhanced insight into the thermoelectric features of KTiAl and KYC compounds. These results demonstrate that KTiAl and KYC are promising materials for thermoelectric applications. As described in Fig. 7, the Z_T values are between 0.01 and 0.81 for KTiAl, and 0.01 and 0.61 for KYC within the temperature interval of 100 to 1000 K. It was observed that Z_T increased to a peak of 0.81 and 0.61 for KTiAl and KYC at 700 K, beyond this point, Z_T declines to 0.70 and 0.48 as the temperature increases to 1000 K. The values around 700 K are noteworthy, as they approach unity, which is the ideal value of Z_T for thermoelectric material. The elevated Z_T values of these compounds underscore their use in thermoelectric power generation. These materials can proficiently convert waste heat into electrical energy, which can be utilized to energize diverse equipment and systems. Further research and development could yield even greater Z_T values for these materials, enhancing their appeal for practical applications. The Z_T values obtained in this study are comparable to other known half-Heusler

compounds, including ScRhTe (0.63) (Singh, 2017), KMnSn and KMnPb (0.70 and 0.76) (Gurunani & Gupta, 2025b), and RbCrC (0.89) (Hammou *et al.*, 2020).

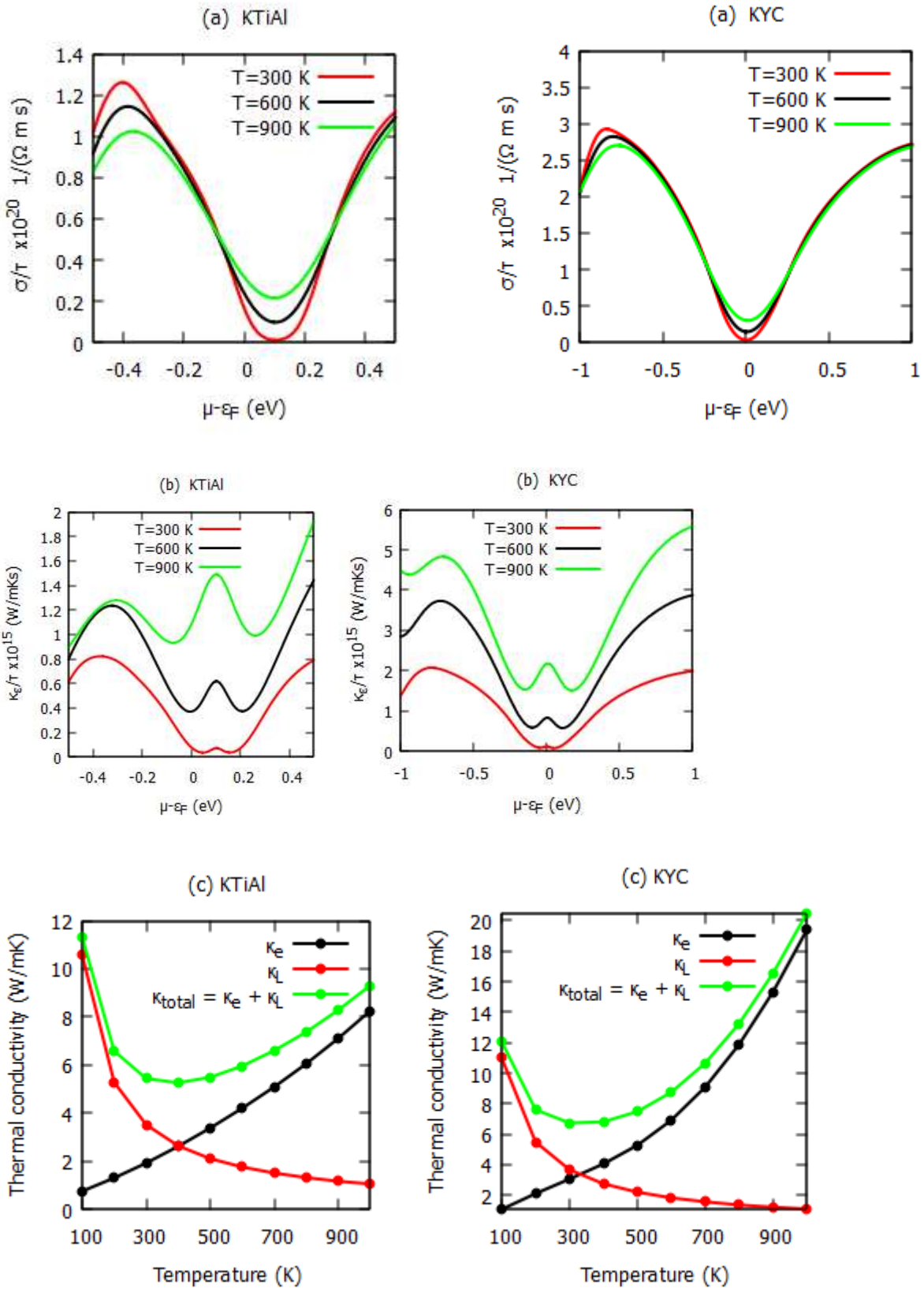


Figure 5. Chemical potential (μ) dependence of the (a) electrical conductivity (b) electronic thermal conductivity and (c) temperature dependence of thermal conductivity for KTiAl and KYC.

Table 4. Computed transport properties for KTiAl and KYC at ambient temperature (300 K)

Alloy	$\boldsymbol{\sigma(\Omega m)^{-1}}$	**S(V/K)**	$\boldsymbol{\kappa_{total}}$**(W/mK)**	**ZT**
KTiAl	3.93×10^{5}	119.3×10^{-6}	5.44	0.31
KYC	4.84×10^{5}	91.31×10^{-6}	6.73	0.18

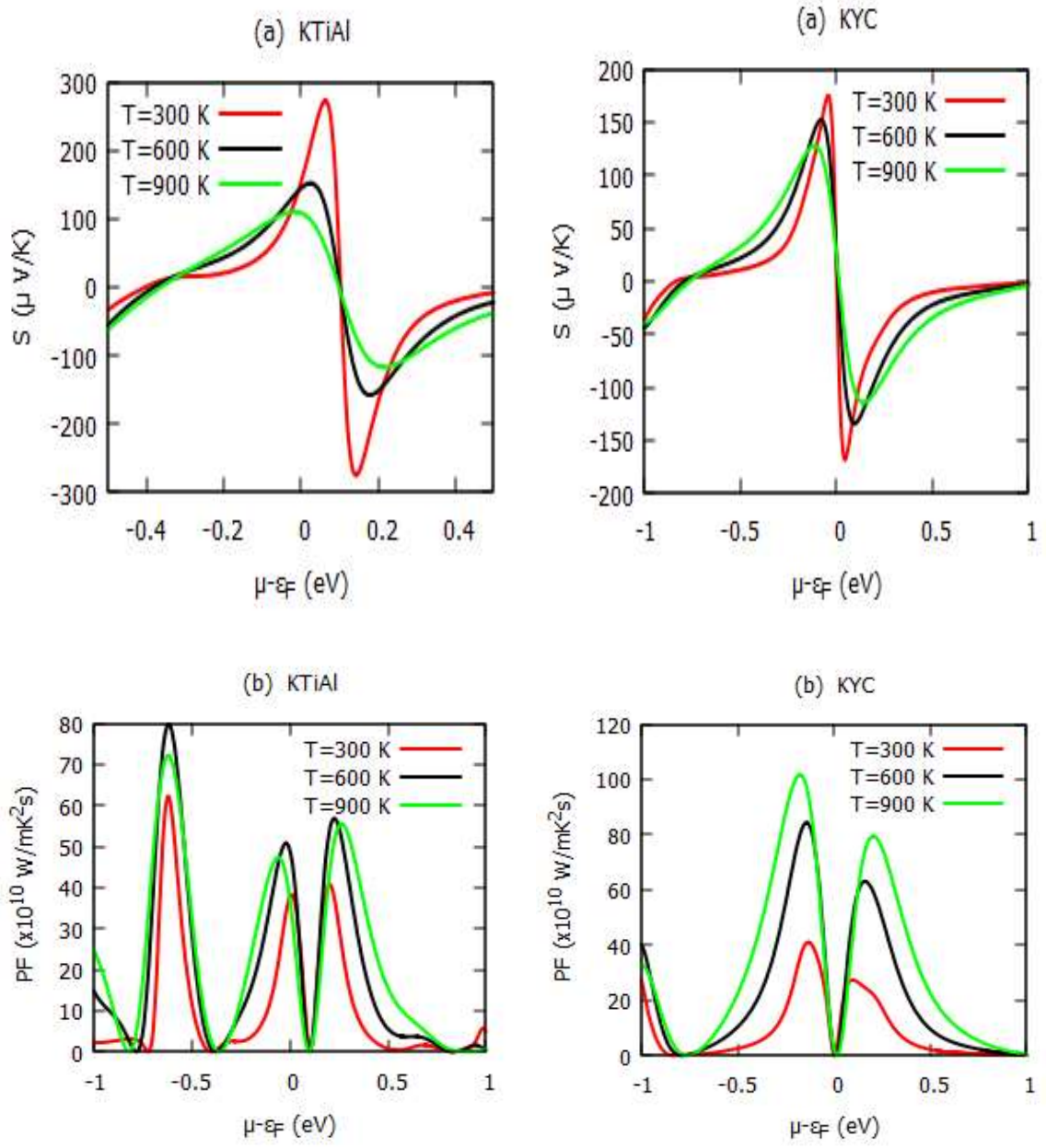


Figure 6. Chemical potential (μ) dependence of the (a) Seebeck coefficient (b) power factor for KTiAl and KYC at different

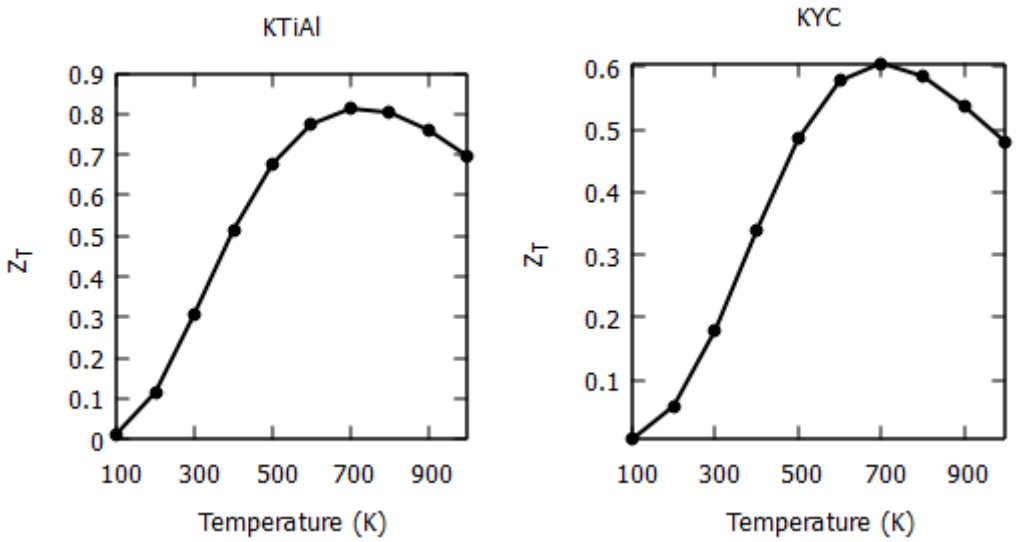


Figure 7. Temperature dependence of the figure of merit (Z_T) for KTiAl and KYC.

4. CONCLUSION

In this study, a systematic first-principles computational assessment was successfully conducted to investigate the structural, electronic, mechanical, and thermoelectric properties of KTiAl and KYC half-Heusler compounds for sustainable energy conversion applications. Volume optimization calculations across the α, β, and γ atomic configurations established that the type γ-phase is the energetically most stable structure for both alloys. Elastic constant analysis confirmed that both materials satisfy the Born stability criteria, demonstrating strong mechanical resilience. Furthermore, evaluated parameters such as the Pugh ratio ($B/G > 1.75$) and positive Cauchy pressure ($C_p > 0$) definitively classify both KTiAl and KYC as ductile materials, indicating their capability to withstand plastic deformation without brittle fracture under high-temperature structural strain. Electronic structure calculations utilizing the highly accurate modified Becke-Johnson (mBJ) exchange-correlation potential revealed that both compounds are non-magnetic, direct bandgap semiconductors. The calculated bandgaps are 0.15 eV for KTiAl and 0.84 eV for KYC, where the Ti-*d* and Y-*d* states provide the dominant contributions near the Fermi level, respectively. This narrow-bandgap nature is highly advantageous for preventing premature thermal carrier excitations while maintaining robust electrical transport capabilities.

Thermoelectric analysis performed via semi-classical Boltzmann transport theory indicated that the electronic transport properties are highly sensitive to temperature and chemical potential adjustments. Under the constant relaxation time approximation, the power factor optimized dramatically at elevated temperatures. Accounting for both electronic and lattice thermal conductivities, the latter derived via Slack's equation, the dimensionless figure of merit (Z_T) was found to rise evidently with temperature. Specifically, the maximum (Z_T) values achieved near 700 K were approximately 0.81 for KTiAl and 0.61 for KYC. These values approach the unity threshold ideal for commercial thermoelectric performance.

In summary, the combined traits of structural stability, excellent mechanical

ductility, narrow direct bandgaps, and high figure of merit values position KTiAl and KYC as exceptionally promising, low-cost, and environmentally benign semiconductor candidates for medium-to-high-temperature waste heat recovery and green energy technologies. Future experimental syntheses and doping strategies are highly encouraged to further suppress lattice thermal conductivity and unlock the full potential of these potassium-based half-Heusler alloys.

Conflicts of interest

The authors declared that there is no conflict of interest.

Acknowledgments

The author(s) acknowledge(s) the Editor in chief and the Reviewers for their selfless services to improve this research work.

REFERENCES

Abu-Farsakh, H., & Qteish, A. (2022). Performance of the modified Becke–Johnson potential employing the pseudopotential plane-wave approach for band structure calculations. *Computational Materials Science*, *208*, 111324. https://doi.org/10.1016/J.COMMATSCI.2022.111324

Achir, B., Bendahma, F., Mehtougui, N., Mana, M., Bentata, S., Benderdouche, N., Righi, A., & Lantri, T. (2026). Unveiling the structural, vibrational, elastic, optoelectronic and thermoelectric characteristics of alkali-yttrium based half-Heusler alloys XYC (X= K, Rb, Cs). *Indian Journal of Physics*, 1–17.

Al-Douri, Y., & Ameri, M. (2025). Physical studies of spintronics-based Heusler alloys. In *Critical Reviews in Solid State and Materials Sciences* (Vol. 50, Number 2). https://doi.org/10.1080/10408436.2024.2407463

Baroni, S., Bonini, N., Calandra, M., Car, R., Cavazzoni, C., Ceresoli, D., Chiarotti, G. L., Cococcioni, M., Dabo, I., Fabris, S., Fratesi, G., Gerstmann, U., Kokalj, A., Lazzeri, M., Martin-Samos, L., Mazzarello, R., Paolini, S., Paulatto, L., Sclauzero, G., … Wentzcovitc, R. M. (2009). QUANTUM ESPRESSO: a modular and open-source software project for quantum simulations of materials. *Journal of Physics: Condensed Matter*, *21*(39).

Berri, S. (2022). Thermoelectric properties of A2BCl6: A first principles study. *Journal of Physics and Chemistry of Solids*, *170*, 110940. https://doi.org/10.1016/J.JPCS.2022.110940

Blaha, P., Schwarz, K., Tran, F., Laskowski, R., Madsen, G. K. H., & Marks, L. D. (2020). WIEN2k: An APW+lo program for calculating the properties of solids. *Journal of Chemical Physics*, *152*(7). https://doi.org/10.1063/1.5143061

Casper, F., Graf, T., Chadov, S., Balke, B., & Felser, C. (2012). Half-Heusler compounds: Novel materials for energy and spintronic applications. In *Semiconductor Science and Technology* (Vol. 27, Number 6). https://doi.org/10.1088/0268-1242/27/6/063001

Chand, P., Kumar, D., & Mohan, L. (2025). Enhanced optoelectronic and thermoelectric properties of half Heusler compounds KXSb (X = Be, Mg, Ca and Sr): A first principle study. *Journal of Physics and Chemistry of Solids*, *196*, 112345. https://doi.org/10.1016/J.JPCS.2024.112345

Coyle, E. D., & Simmons, R. A. (2014). Understanding the Global Energy Crisis. In *Understanding the Global Energy Crisis*.

https://doi.org/10.2307/j.ctt6wq56p

Gruhn, T. (2010a). Comparative ab initio study of half-Heusler compounds for optoelectronic applications. *Physical Review B - Condensed Matter and Materials Physics*, *82*(12). https://doi.org/10.1103/PhysRevB.82.125210

Gruhn, T. (2010b). Comparative ab initio study of half-Heusler compounds for optoelectronic applications. *Physical Review B - Condensed Matter and Materials Physics*, *82*(12). https://doi.org/10.1103/PhysRevB.82.125210

Guo, D., Ran, Y., He, J., Zhang, L., Zhou, D., Yu, Z., & Tai, K. (2025). Enhanced Near-Room-Temperature Thermoelectric Performance of Mg3Bi2 Through Ag Doping. *Acta Metallurgica Sinica (English Letters)*, *38*(10). https://doi.org/10.1007/s40195-025-01907-0

Gurunani, B., & Gupta, D. C. (2025a). First-principles investigation of thermoelectric performance in KMnZ (Z = Sn, Pb) half-Heusler alloys. *RSC Advances*, *15*(7). https://doi.org/10.1039/d5ra00220f

Gurunani, B., & Gupta, D. C. (2025b). First-principles investigation of thermoelectric performance in KMnZ (Z = Sn, Pb) half-Heusler alloys. *RSC Advances*, *15*(7). https://doi.org/10.1039/d5ra00220f

Hammadache, O., Mesbah, S., Houari, M., Khelifa-Kerfa, K., Benghanem, M., Lantri, T., & Belarbi, B. (2024). KCaAs and KCaP: promising half-Heusler compounds for UV protection and thermoelectric applications. *Physica Scripta*, *99*(11). https://doi.org/10.1088/1402-4896/ad8191

Hammou, M., Bendahma, F., Mana, M., Terkhi, S., Benderdouche, N., Aziz, Z., & Bouhafs, B. (2020). Thermoelectric and Half-Metallic Behavior of the Novel Heusler Alloy RbCrC: Ab initio DFT Study. *SPIN*, *10*(4). https://doi.org/10.1142/S2010324720500290

Haro, A. F. (2025). Generalized Gradient Approximation Made Simple: Theoretical Review: Aproximación Generalizada del Gradiente Simplificada: Revisión Teórica. *Multidisciplinary Latin American Journal (MLAJ)*, *3*(3).

Hashmat, Z., Ko, C., Rahman, A. U., Tumelero, M. A., Lazo, M., El-Bahy, S. M., & Magalhaes, S. G. (2025). First-principles prediction of semiconducting half-Heusler KXP compounds (X: Ca, Sr, Ba) for optoelectronic and photocatalytic applications. *Scientific Reports*, *15*(1). https://doi.org/10.1038/s41598-025-32052-4

Khaliq, A., Zhou, X., Chai, H. Y., Ali, M., Wu, H., Gassab, O., Liu, H., Xiao, D., Yang, X. G., & Du, S. (2024). Illumination Induced Negative Differential Resistance in InGaAs Avalanche Photodiode. *IEEE Access*, *12*. https://doi.org/10.1109/ACCESS.2024.3383836

Khatri, P., Lamichhane, S., & Adhikari, N. P. (2026). Elucidation of electronic structure and thermoelectric properties of I–III–IV class half Heusler compounds with eight valence electron count. *Journal of Physics and Chemistry of Solids*, *208*, 113132. https://doi.org/10.1016/J.JPCS.2025.113132

Kumar, D., & Chand, P. (2023). Enhanced optical and thermoelectric properties of Ti doped half - Heusler alloy NbRuP: A first principles study. *Solid State Communications*, *366–367*, 115179. https://doi.org/10.1016/J.SSC.2023.115179

Madsen, G. K. H., Carrete, J., & Verstraete, M. J. (2018). BoltzTraP2, a program for interpolating band

structures and calculating semi-classical transport coefficients. *Computer Physics Communications*, *231*, 140–145. https://doi.org/10.1016/J.CPC.2018.05.010

Mahmud, S., Atik, M. A. U. Z., Mostakim, M. N., Tarekuzzaman, M., & Hasan, M. Z. (2024). Investigation of direct small bandgap Cs2AuInX6 (X= F/Cl) double perovskites for energy harvesting technology employing DFT. *Computational Condensed Matter*, *40*, e00950. https://doi.org/10.1016/J.COCOM.2024.E00950

Morris, J. W., & Krenn, C. R. (2000). The internal stability of an elastic solid. *Philosophical Magazine A: Physics of Condensed Matter, Structure, Defects and Mechanical Properties*, *80*(12). https://doi.org/10.1080/01418610008223897

Murnaghan, F. D. (1944). The Compressibility of Media under Extreme Pressures. *Proceedings of the National Academy of Sciences*, *30*(9). https://doi.org/10.1073/pnas.30.9.244

Nenuwe, N. O., & Omagbemi, O. W. (2026). First Principles Investigation of PtTaAl Half-Heusler: Structural, Electronic, Optical, and Thermoelectric Properties for High-Performance Medium-to-High-Temperature Clean Energy and Waste-Heat Recovery Applications. *Journal of Superconductivity and Novel Magnetism*, *39*(3). https://doi.org/10.1007/s10948-026-07189-6

Nenuwe, N. O., & Yebovi, A. S. (2024). Predictive analysis of a new FeVTe alloy from first principles: An excellent choice for thermoelectric applications. *Computational Condensed Matter*, *38*. https://doi.org/10.1016/j.cocom.2024.e00882

Ole Rolser Christer Tryggestad, N. S. (2019). Global Energy Perspective 2019 : Reference Case. *Energy Insights by McKinsey & Company*, (January).

Özdoğan, K., & Galanakis, I. (2024). Interplay Between Structural, Electronic, and Magnetic Properties in the d0-d Semi-Heusler Compounds; the Case of the K-Based Compounds. *Solids*, *5*(4). https://doi.org/10.3390/solids5040036

Panday, K. R., Gaire, G., Regmi, N., Khatri, P., & Adhikari, N. P. (2026). Unveiling the Thermoelectric Properties of Some Bismuth Based Half Heuslers: A First-Principles Perspective. *Advanced Theory and Simulations*, *9*(1). https://doi.org/10.1002/adts.202501816

Park, H., Park, O., Lee, C., Kim, Y. W., Kim, S. il, & Kim, H. S. (2025). Influence of Band Gap Enlargement on Thermoelectric Performance in Cu0.008Bi2Te3. *Korean Journal of Materials Research*, *35*(2). https://doi.org/10.3740/MRSK.2025.35.2.96

Rogl, G., & Rogl, P. (2017). Skutterudites, a most promising group of thermoelectric materials. In *Current Opinion in Green and Sustainable Chemistry* (Vol. 4). https://doi.org/10.1016/j.cogsc.2017.02.006

Saikia, D., Sharma, R., El-Rayyes, A., & Alshihri, A. A. (2025). Exploring the Electronic and Thermoelectric properties of FeMnZ (Z = P, As) Half-Heusler Alloys for Spintronics: A DFT Insight. *Journal of Electronic Materials*. https://doi.org/10.1007/s11664-025-12599-8

Schwarz, K., Blaha, P., & Madsen, G. K. H. (2002). Electronic structure calculations of solids using the WIEN2k package for material sciences. *Computer Physics Communications*, *147*(1–2), 71–76. https://doi.org/10.1016/S0010-4655(02)00206-0

Seebeck, T. J. (2003). “Magnetische Polarisation der Metalle und Erze

durch Temperatur-Differenz" (Magnetic polarization of metals and minerals by temperature differences), Abhandlungen der Königlichen Akademie der Wissenschaften zu Berlin. *Treatises of the Royal Academy of Sciences in Berlin*.

Sharma, P. K., Senguttuvan, T. D., Sharma, V. K., & Chaudhary, S. (2021). Revisiting the thermoelectric properties of lead telluride. In *Materials Today Energy* (Vol. 21). https://doi.org/10.1016/j.mtener.2021.100713

Shi, Y., Sturm, C., & Kleinke, H. (2019). Chalcogenides as thermoelectric materials. *Journal of Solid State Chemistry*, *270*. https://doi.org/10.1016/j.jssc.2018.10.049

Shrivastava, D., & Sanyal, S. P. (2019). Theoretical study of structural, electronic, phonon and thermoelectric properties of KScX (X=Sn and Pb) and KYX (X=Si and Ge) half-Heusler compounds with 8 valence electrons count. *Journal of Alloys and Compounds*, *784*, 319–329. https://doi.org/10.1016/j.jallcom.2019.01.050

Singh, S. (2017). Assessing the thermoelectric properties of ScRhTe half-heusler compound. *Computational Condensed Matter*, *13*. https://doi.org/10.1016/j.cocom.2017.10.002

Slack, G. A. (1973). Nonmetallic crystals with high thermal conductivity. *Journal of Physics and Chemistry of Solids*, *34*(2). https://doi.org/10.1016/0022-3697(73)90092-9

Subramani, A., Vairapperumal, T., Srinivasan, M., & Klinton Brito, K. (2025). Novel TiPdC Half-Heusler Alloys with High Thermoelectric Performance for High-Grade Waste Heat Energy Harvesting. *Physica Status Solidi (B): Basic Research*, *262*(6). https://doi.org/10.1002/pssb.202400577

Tran, F., & Blaha, P. (2009). Accurate band gaps of semiconductors and insulators with a semilocal exchange-correlation potential. *Physical Review Letters*, *102*(22). https://doi.org/10.1103/PhysRevLett.102.226401

Tritt, T. M., Littleton, R. T., & Lowhorn, N. D. (2001). Investigation of the thermoelectric properties of the pentatelluride system MTe5-xSex (M=Hf,Zr) for potential low temperature refrigeration applications. *Pricm 4: Forth Pacific Rim International Conference on Advanced Materials and Processing, Vols I and Ii*.

Tyuterev, V. G., & Vast, N. (2006). Murnaghan's equation of state for the electronic ground state energy. *Computational Materials Science*, *38*(2). https://doi.org/10.1016/j.commatsci.2005.08.012

Ullah, Z., Khan, R., Khan, M. A., Otaibi, S. Al, Althubeiti, K., Soliyeva, M., Elboughdiri, N., & Raziq, F. (2026). First principles insights into the electronic, optical, and thermoelectric properties of Cu2ZnSnS4 for energy conversion applications. *Results in Physics*, *80*. https://doi.org/10.1016/j.rinp.2025.108561

Wu, Z., & Cohen, R. E. (2006). More accurate generalized gradient approximation for solids. *Physical Review B - Condensed Matter and Materials Physics*, *73*(23). https://doi.org/10.1103/PhysRevB.73.235116

Xu, X., Dong, Y., Hu, Q., Si, N., & Zhang, C. (2024). Electrochemical Hydrogen Storage Materials: State-of-the-Art and Future Perspectives. In *Energy and Fuels* (Vol. 38, Number 9). https://doi.org/10.1021/acs.energyfuels.3c05138

Zhang, X., & Zhao, L. D. (2015).

Thermoelectric materials: Energy conversion between heat and electricity. In *Journal of Materiomics* (Vol. 1, Number 2). https://doi.org/10.1016/j.jmat.2015.01.001